Metals **2012**, *2*, 22-40; doi:10.3390/met2010022

OPEN ACCESS

metals

ISSN 2075-4701

www.mdpi.com/journal/metals/

Review

Nanocrystalline Metal Hydrides Obtained by Severe Plastic Deformations

Jacques Huot

Université du Québec à Trois-Rivières, 3351 des Forges, Trois-Rivières, Québec, G9A 5H7, Canada; E-Mail: jacques.huot@uqtr.ca; Tel.: +1-819-376-5011 (ext. 3576); Fax: +1-819-376-5164

Received: 30 November 2011; in revised form: 27 December 2011 / Accepted: 27 December 2011 / Published: 10 January 2012

Abstract: It has recently been shown that Severe Plastic Deformation (SPD) techniques could be used to obtain nanostructured metal hydrides with enhanced hydrogen sorption properties. In this paper we review the different SPD techniques used on metal hydrides and present some specific cases of the effect of cold rolling on the hydrogen storage properties and crystal structure of various types of metal hydrides such as magnesium-based alloys and body centered cubic (BCC) alloys. Results show that generally cold rolling is as effective as ball milling to enhance hydrogen sorption kinetics. However, for some alloys such as $TiV_{0.9}Mn_{1.1}$ alloy ball milling and cold rolling have detrimental effect on hydrogen capacity. The exact mechanism responsible for the change in hydrogenation properties may not be the same for ball milling and cold rolling. Nevertheless, particle size reduction and texture seems to play a leading role in the hydrogen sorption enhancement of cold rolled metal hydrides.

Keywords: metal hydrides; severe plastic deformation; cold rolling; BCC alloys; magnesium-based alloys

1. Introduction

The effects of mechanical deformation on the hydrogen storage behavior of metal hydrides have been intensively studied in the last decade. Mechanochemistry offers the possibility to conduct various reactions, including the synthesis of substances in the nanocrystalline and amorphous states, at low temperatures without dissolution or fusion of the reactants. Forty years after the pioneering works of Benjamin [1] the mechanochemical treatment of substrates in producing new thermodynamically

stable and metastable materials, often non achievable by traditional methods, is well established and has been applied by the industry. However, knowledge about the physical mechanisms operating during the mechanochemical treatment is still very limited due to serious difficulties in quantifying this complex process [2].

A common result of high energy Ball Milling (BM) and Severe Plastic Deformation (SPD) and SPD is the formation of nanocrystalline or amorphous structure along with formation of defects and increase of grain boundaries. In many systems such structure leads to enhanced mechanical and chemical properties. For example, defects could act as nucleation point for a chemical reaction (such as hydrogenation) while grain boundaries could act as fast diffusion pathways. Therefore, these techniques are particularly attractive for synthesis and preparation of metal hydrides materials. In this paper a few selected SPD techniques (High Pressure Torsion, Equal Channel Angular Pressing, and Cold Rolling) will be discussed. Each of these methods will be described and a few specific systems will be discussed by comparing ball milling with SPD techniques.

2. Techniques

There are many SPD techniques. In this paper we will discuss only the three mostly applied to metal hydrides namely High pressure Torsion (HPT), Equal Angular Chanel Pressing (ECAP), and Cold Rolling (CR) with an emphasis on the last one.

2.1. High Pressure Torsion

Compare to other SPD techniques, High Pressure Torsion (HPT) is a relatively simple and quick processing technique. It is also very efficient to produce small grain size [3]. The principle of HPT is schematically illustrated in Figure 1.

Figure 1. Schematic illustration of High Pressure Torsion (HPT). Adapted from reference [4].

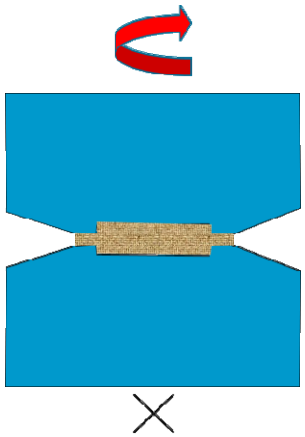

The sample, generally in the form of a thin disk, is located between the piston and the anvil within a cavity. A hydrostatic pressure is applied and plastic torsional straining is achieved by rotation of the piston. The diameter of the cylindrical cavities and the initial diameter of the HPT sample are identical. However, the sum of both depths of the cavities is somewhat smaller than the initial height of the HPT sample. This implies that during loading a small amount of the material will flow in the ring shaped

region between the two anvils. The friction in this region confines the free flow of the material out of the HPT tool and leads to a back pressure and induces a defined hydrostatic pressure within the processing zone. More details of this technique could be found in reference [4].

2.2. HPT Effects on Metal Hydrides

Application of HPT to hydrogen storage materials is relatively new. One of such study was performed by Kusadome *et al.* on $MgNi_2$ alloy [5] which does not usually absorb hydrogen. The crystallite size of $MgNi_2$ phase changed from more than 100 nm before HPT processing ton about 20 nm after 10 HPT revolutions. Moreover, the HPT processing introduced a substantial strain into the material, and $MgNi_2$ became a weak hydrogen absorber (0.1 wt.%) with hydrogen accumulating in grain boundaries of the alloy [5].

A certain similarity between HPT and ball-milling can be made based on the recent work by Leiva *et al.*, who detected the formation of a metastable phase γ-MgH_2 and a substantial reduction of crystallite sizes from 30 to 20 nm while using HPT to consolidate the metal hydride powder [6]. Previously, the formation of γ-MgH_2 upon mechanical processing was reported for and chiefly associated with high-energy ball-milling [7]. HTP has also been used for Mg-Fe and Mg-Ni compounds. In the case of Mg–Fe system, Lima *et al.* were able to synthesize the ternary complex Mg_2FeH_6 and the binary MgH_2 hydrides by hydrogenation treatment at 350 °C, at 3 MPa during 24 h [8]. However, the hydride formation was not complete because after hydrogenation XRD pattern showed the presence of Mg, Fe, MgH_2 and Mg_2FeH_6. Révész *et al.* subjected 7Mg + 3Ni powders to ball milling followed by High Pressure Torsion (HPT) [9]. The result was a microstructural refinement accompanied with the creation of straining and/or lattice defects. Absorption kinetic data indicated that the maximum H-absorption capacity was increased by 30–50% after HPT due to the creation of new possible hydrogen absorption sites at the grain boundaries and at lattice defects. On the other hand, the initial absorption rate was somewhat decreased due to HPT [9].

2.3. Equal Channel Angular Pressing

2.3.1. Description of the Technique

In the Equal Channel Angular Pressing (ECAP) technique, severe plastic deformations are introduced into a material by forcing a sample (billet) with a piston through a die consisting of two channels of equal cross-section, which intersect at an angle (Φ) between 90° and 120° [10] (see Figure 2). The outer arc of curvature where the two channels intersect is labelled Ψ. Since the billet assumes the form and the cross-section of the die, it can be repeatedly processed to increase the microstrain and reduce the size of crystallites in the material. ECAP is quite efficient in processing metals and allows to produce porosity-free materials with average crystallite sizes between 2 μm and 100 nm in substantial quantities with lower concentration of impurities and at a lower cost than ball-milling [11]. Through the grain refinement process, the proportion of high angle grain boundary (HAGB) increases due to dislocations recovery [12]. Texture could also be introduced by this process.

Figure 2. Schematic illustration of Equal Channel Angular Pressing (ECAP).

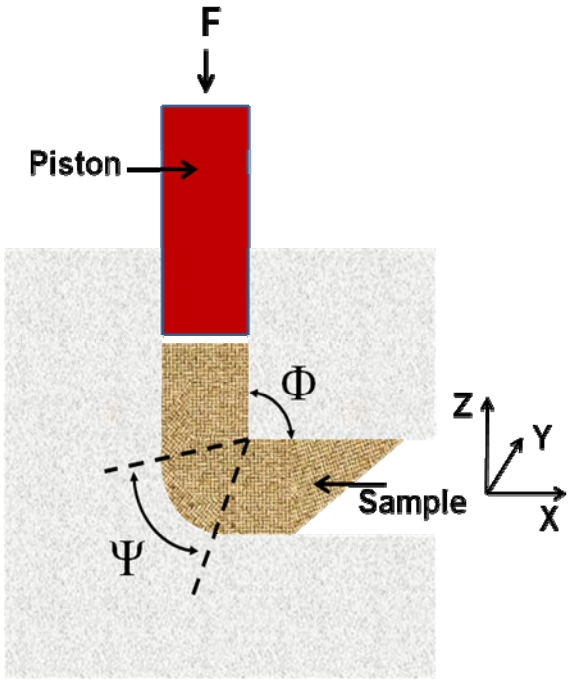

2.3.2. ECAP Effects on Metal Hydrides

Skripnyuk *et al.* have investigated the effect of ECAP on the hydrogen storage behavior of Mg-based alloys [13–16]. First, they investigated the hydrogenation properties of a readily available structural alloy ZK60 of the composition Mg–4.95 wt.% Zn–0.71 wt.% Zr [13]. The alloys were processed by high energy ball milling (HEBM), ECAP, and a combination of ECAP and HEBM. The ECAP processing was made through route A with eight passes at 250–300 °C and one additional pass at room temperature. They found that after ECAP/HEBM treatment the hysteresis in the pressure-composition isotherm completely disappears. However, the most important effect of processing was on the hydrogen desorption kinetics.

Skripnyuk *et al.* also investigated the hydrogenation properties of magnesium doped with carbon nanotubes (CNT). When HEBM is used to synthesize Mg–CNT mixtures destruction of CNT is happening after a relatively short time of milling. Their idea was to use ECAP to get a good contact between Mg and CNT [16]. They found that ECAP led to a slow down of absorption/desorption at the initial stages of the processes, and to their acceleration at the later stages. The complex effect of ECAP on the hydrogenation kinetics of the composite is considered to be associated with two competing factors, namely, a decrease in hydrogen diffusivity along the CNTs due to their failure and kinking, and concurrent enhancement of the hydrogen diffusion kinetics in the Mg matrix [16].

Løcken *et al.* used ECAP and HEBM to process the ternary eutectic Mg–Mg_2Ni–$MmMg_{12}$ (72 wt.% Mg–20 wt.% Ni–8 wt.% Mm, Mm = mischmetal) [17]. Eight ECAP passes at 400 °C (route B_C) gave an improvement in the hydrogen absorption and desorption rates. However, HEBM gave an even larger improvement and reduced the absorption and desorption times to one third of those of the as-cast alloy.

Recently, Krystian *et al.* performed ECAP on commercial magnesium alloy ZK60 and were able to decrease the grain size down to 250 nm—the smallest value ever achieved by this technique [18]. The hydrogen storage capacity was measured to be 6.6 wt.% and rapid hydrogen desorption kinetics of less than 5 min at 623 K was registered. The long term durability of the material was proven in a cyclic sorption/desorption test up to 1000 cycles and no deterioration in storage capacity or in kinetics was observed which is exceptional for nanomaterials for hydrogen storage.

2.4. Cold Rolling

2.4.1. Description of the Technique

In cold rolling (CR) a sheet of metal is introduced between rollers where it is compressed and squeezed (Figure 3). The amount of strain introduced by CR determines the hardness and other properties of the finished product.

Figure 3. Schematic illustration of Cold Rolling (CR).

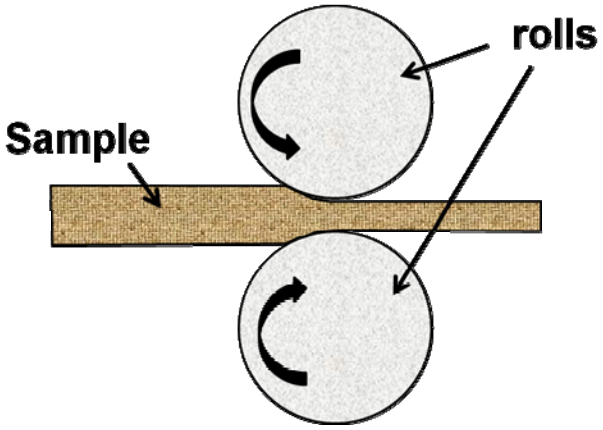

Usually, rolling is classified according to the processing temperature as compared with the metal re-crystallization temperature:

- Hot Rolling (HR) is when the process is carried out at a temperature exceeding the re-crystallization temperature of the rolled material and;
- Cold Rolling (CR) is when rolling temperature is below re-crystallization temperature.

To our knowledge, up to now only cold rolling has been used for synthesis and preparation of metal hydrides. Therefore, only this technique will be discussed.

2.4.2. CR Effects on Ti-Based Alloys

Basically, up to now, the effect of cold rolling on hydrogen sorption properties has been investigated only for two systems: Mg-based compounds and Ti-based alloys. In the case of Ti-based alloys, one of the first investigations of the effect of cold rolling on metal hydrides was made by Zhang *et al.* who studied the effect of deformations on hydrogen sorption behavior of Ti–22Al–27Nb alloy [19,20]. They found that the first hydrogenation (activation) of the cold rolled alloys was much faster than that of the unprocessed samples. Unfortunately, the positive effect of CR processing

disappeared after a few hydrogenation cycles as the material returned to its initial state. In a recent study of the Ti–Al–Nb system, Patselov *et al.* observed that a 28% deformation (engineering strain) by cold rolling resulted in a 25% increases of hydrogen capacity in comparison with as-cast alloy of the same composition [21]. At this level of deformation the material has a lot of curvilinear intersect dislocations including tangled configurations. These features most likely play a role in the hydrogen enhancement but, as for higher level of strain the capacity decreases, there is probably a more complex explanation of beneficial effect of deformation on the hydrogen absorption behavior [21].

Couillaud *et al.* investigated the effect of cold rolling and ball milling on $TiV_{1.6}Mn_{0.4}$ alloy [22]. The effect of extended cold rolling as well as energetic ball milling was a slight reduction of crystalline size (from 17 nm to 13 nm) and lattice parameter (from 0.3082 nm to 0.3061 nm) but no change in the crystal structure. Unfortunately, neither ball milled sample nor cold rolled sample absorb hydrogen even after 10 cycles of hydrogen pressurization (10 MPa) and vacuum at 423 K. The reason for this significant loss of hydrogen capacity is still unknown. As ball milling was performed in argon oxygen contamination is unlikely to have occurred.

The system Ti-Cr has been investigated by Amira *et al.* who compared the effect of cold rolling and ball milling on as-cast $TiCr_x$ (x = 2, 1.8 and 1.5) [23]. They showed that $TiCr_x$ transforms from a mixture of C14 and C15 Laves phases to a metastable BCC phase after 5 h of ball milling under argon. Cold rolling did not lead to the formation of a metastable BCC phase but only to the reduction of $TiCr_x$ size particles under 20 nm. Surprisingly, despite the discrepancies in crystal structures, the hydrogen absorption/desorption curves of cold rolled and ball milled samples at 323 K were quite similar.

2.4.3. CR Effects on Magnesium-Based Alloys

Because of its high hydrogen storage capacity, magnesium is interesting for hydrogen storage applications. However, because of the limited number of slip planes, work hardening occurs rapidly after only a few rolling passes. Thus, upon rolling a magnesium foil will quickly break up in small pieces and made further rolling more and more difficult. Nevertheless, for hydrogen storage applications mechanical integrity is not so important. In fact, after a few hydrogenations many metal hydrides turn into powder because of the important decrepitation due to the significant volume change during hydrogenation. Consequently, cold rolling of magnesium and magnesium alloys have been actively investigated.

Ueda *et al.* were the first to try to synthesize a metal hydride (Mg_2Ni) using cold rolling of raw elements followed by heat treatment [24]. For stoichiometry 2Mg + Ni, single phase Mg_2Ni was obtained, and the sample could be completely hydrogenated to Mg_2NiH_4. The formation of Mg_2Ni was explained by interdiffusion between Mg and Ni during heat treatment [24]. Pednault *et al.* also investigated the Mg–Ni system for electrochemical applications [25,26]. They investigated the structural and electrochemical evolution of 2Mg–Ni cold-rolled samples as a function of the number of rolling passes as well as heat treatment. It was found that nanocrystalline Mg_2Ni alloy can be obtained by an appropriate three step process involving rolling, heat treatment and rolling again. The best result was obtained by first rolling 90 times, followed by a heat treatment at 400 °C for 4 h and roll again 20 times. The resulting material had a Mg_2Ni phase with a crystallite size of 12 nm and displayed an

initial discharge capacity of 205 mAh g^{-1}, which is quite similar to that obtained with ball-milled Mg_2Ni alloy [25].

In the case of Mg–Pd system, Dufour and Huot studied the effect of adding 2.5 at.% of Pd to Mg by cold rolling and by ball milling [27]. Figure 4 shows the morphology of laminated and ball-milled samples. Palladium is evenly distributed in both samples but the particle size is almost one order of magnitude bigger in the laminated compound compared to the ball milled one. Nevertheless, as shown in Figure 5, the first hydrogenation (activation) of laminated sample is much faster than shows a much shorter activation time compared to a ball-milled sample. Moreover, when the cold rolled sample was subjected to five cycles of hydrogen absorption/desorption, taken out and stored in air for one month the activation was still faster than the ball milled sample. This shows that cold rolled samples have a much better resistance to air contamination. This is probably due to the much smaller specific surface area of a cold rolled material compared to its ball milled counterpart.

Figure 4. Scanning electron micrographs from backscattered electrons of Mg–Pd 2.5 at.%: (**A**) after 20 rolling passes and (**B**) after 2 h of ball milling. The white marks are palladium particles. From reference [27].

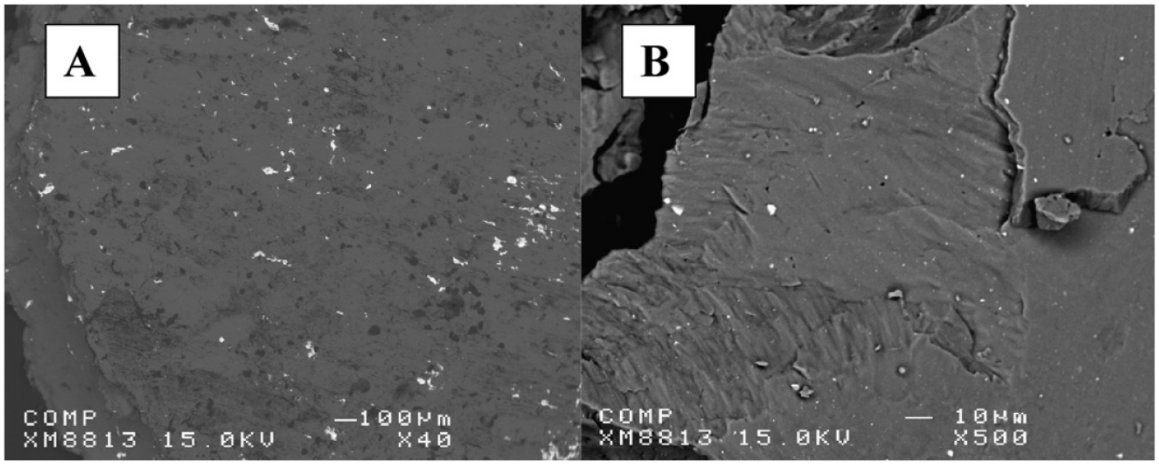

Figure 5. Activation curve of ball milled Mg–Pd 2.5 at.%, cold rolled Mg–Pd 2.5 at.%, and cold rolled pure magnesium. Activation temperature 623 K, pressure 1.3 MPa. CR = cold rolled, BM = ball-milled. From reference [27].

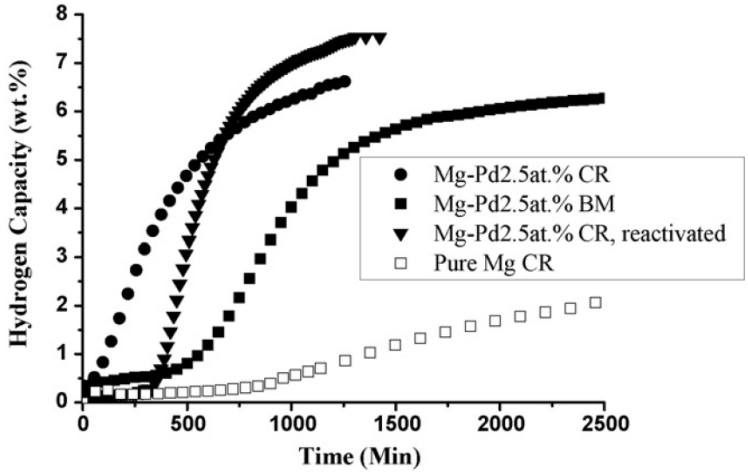

In subsequent investigations, Takeichi *et al.* [28] as well as Dufour and Huot [29] have shown that the alloy Mg_6Pd could be synthesized by cold rolling followed by heat treatment. Other Mg–X systems such as Mg–Ti [30,31], Mg–Al [32], Mg–Cu [28,33], Mg–Fe [6,34] as well as commercial Mg–Zr–Zn alloy [35] have also been investigated.

3. BCC Alloys for Hydrogen Storage

The use of mechano-chemical methods for the synthesis and modification of hydrogen storage materials has generated an enormous amount of reports. In the last 10 years about a thousand papers have been published on the use of ball milling and mechanical alloying for this specific application. Therefore, covering all aspects and systems is out of the scope of the present review. In this section, we focus on the use of mechanochemical methods to tune the microstructure of BCC alloys in order to improve their hydrogenation properties.

A body centered cubic (BCC) structure is a coarse packing structure and has much more interstitial sites than face centered cubic (FCC) and hexagonal close packed (HCP) structures [36]. Thus, BCC alloys are one of the most attractive candidates to obtain high hydrogen storage capacity. Usually, BCC alloys are synthesized by arc melting or induction melting. However, for some compositions an exact stoichiometric compound is difficult to obtain by using these techniques because the elements may have quite different melting temperatures. With mechanical alloying there is in principle no limitation on the nature and number of the raw elements used. For hydrogen storage applications one could distinguish two broad classes of BCC alloys: Ti-based and Mg-based. Each of them is discussed below.

3.1. Ti-Based BCC

BCC alloys of systems Ti–V–Mn and Ti–V–Cr have been intensively studied for hydrogen storage [37–42]. They could also be used as catalyst for magnesium [43]. Hydrogen capacities as high as 3.6 wt.% have been reported for $Ti_{25}V_{40}Cr_{35}$ alloy.

The effect of severe plastic deformation (SPD) on BCC Ti–22Al–27Nb alloy has been investigated by Zhang *et al.* [19,20]. They showed that the first hydrogenation (activation) was much faster for the deformed alloy compared to the as-quenched sample. The deformed alloy had also a faster absorption/desorption kinetics. However, the beneficial effect of deformation was lost after a few hydrogenation cycles. In these studies, SPD was obtained by cold rolling or compression. In the case of cold rolling one rolling was performed at 10.5% and 80% thickness reduction. Some of the 80% rolled specimen were further rolled to 10% thickness reduction in a perpendicular direction with respect to the first rolling.

Huot *et al.* have made a systematic study of the effect of milling on $TiV_{0.9}Mn_{1.1}$ alloy [44]. This composition is interesting to study because the as-cast alloy is a mixture of BCC and C14 phases. Therefore, it is a good system to test the effect of milling on the crystalline change and the interaction between phases. Milling was performed on as-cast alloy as well as on mixtures of elemental powders. Figure 6 shows the effect of milling on as-cast $TiV_{0.9}Mn_{1.1}$.

The presence of NaCl Bragg peaks is explained by the use of a small amount of this salt as an anti-sticking agent. It is clear that, with milling time, the C14 phase vanishes and a FCC phase appears.

From Rietveld refinement it was found that, for the sample milled 80 h, the crystal structure is a mixture of cubic (FCC) solid solution phase and a BCC solid solution. The coexistence of FCC and BCC has been seen in the system Fe–Cu and was explained by an enhanced solubility due to the high dislocation density [45] but this explanation may not be applicable in the present case. From Rietveld refinement it was determined that the crystallite size of the BCC phase goes from 44 nm before milling to 2 nm after 80 h of milling. When milling was performed on the raw elements (Ti, V, and Mn) an identical result was obtained, that is formation of a nanocrystalline alloy composed of BCC and FCC phases [44].

Figure 6. X-ray powder diffraction pattern of arc-melted $TiV_{0.9}Mn_{1.1}$ as a function of milling time. From reference [44].

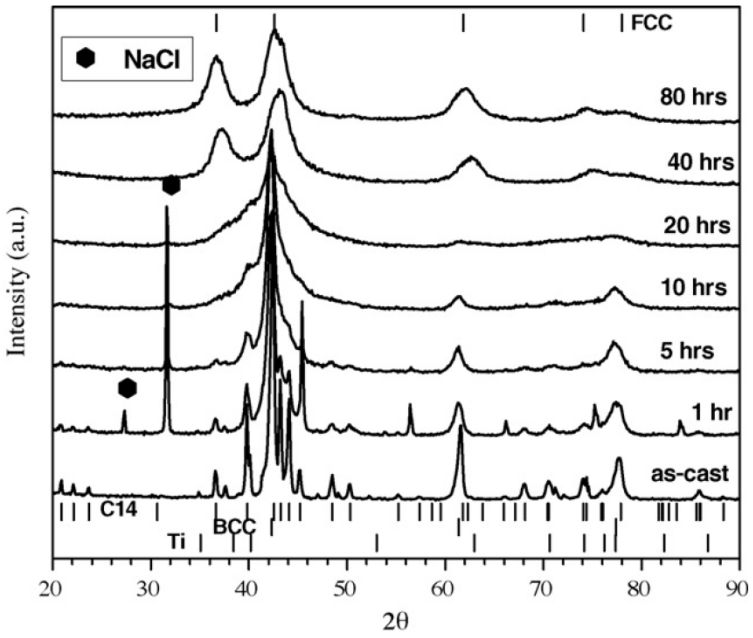

Before measurement of hydrogen storage properties BCC alloys have to be activated. In the present case, the activation was made by cycling between high hydrogen pressure (5 MPa) and vacuum at elevated temperature (up to 250 °C). In Figure 7 the hydrogen absorption and desorption isotherm (23 °C) for arc-melted $TiV_{0.9}Mn_{1.1}$ before and after 80 hours of milling is presented. The maximum capacity of the as melted alloy is 1.9 wt% at 7 MPa which corresponds to a H/M ratio of 0.97. After 80 h of milling, the alloy does not absorb hydrogen up to 7 MPa. Because the as-milled materials present both FCC and BCC phases this means that both of them do not absorb hydrogen. In the case of BCC phase the reason may be reduction of lattice parameters. Iron contamination (even at this low level) may also play a role as shown by Santos *et al.* in Ti–V–Cr system [46].

Singh *et al.* studied the effect of milling on arc melted $Ti_{0.32}Cr_{0.43}V_{0.25}$ alloy [47]. As they used tungsten carbide balls, some contamination was observed after long milling time. Ball milling did not affect the apparent bulk structure of the alloy. Increase of ball milling time resulted in the increase in lattice strain and the decrease in crystallite size, which in turn increased subgrain boundaries. These contamination and microstructural changes caused an important decrease in the hydrogen storage capacity [47].

Amira *et al.* compared the effect of ball milling and cold rolling for Ti–Cr system [23]. Unlike ball milling, cold rolling of $TiCr_x$ (x = 2, 1.8, 1.5) did not lead to the formation of metastable BCC phase. However, cold rolling was found to be effective to form nanocrystalline C14 Laves phase. Hydrogen sorption experiments showed that cold rolled alloys have similar hydrogen sorption properties than their ball milled counterparts despite different crystal structures. This result proves that hydrogen absorption/desorption properties do not depend only of the microstructure.

Figure 7. Pressure–composition temperature (PCT) curve, at 313 K, of arc-melted $TiV_{0.9}Mn_{1.1}$ alloy after 80 h of milling. From reference [44].

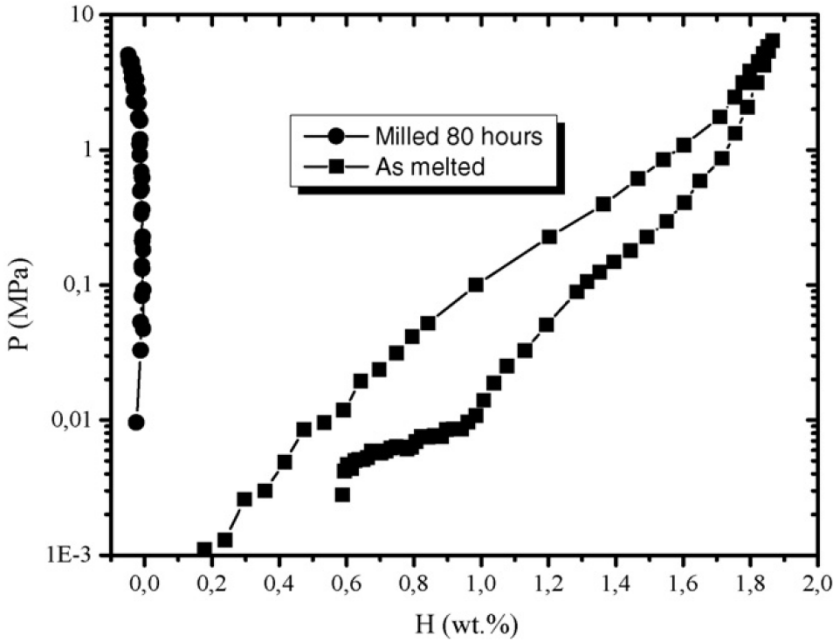

The alloy $TiV_{1.6}Mn_{0.4}$ has been recently investigated by Couillaud *et al.* [22]. The effect of extended cold rolling as well as energetic ball milling was a reduction of crystalline size and lattice parameter but no change in the crystal structure. Figure 8 shows TEM micrographs of $TiV_{1.6}Mn_{0.4}$ alloy in the as-cast, milled, and cold rolled states.

The dark field image shows that all samples are nanocrystalline. The bright field image of the cold rolled sample clearly shows the pile-up of dislocations. The dark field image shows that, contrary to the as-cast and ball milled samples, the crystallites tend to be aligned along dislocations. Figure 9 shows the X-ray diffraction patterns of as-cast, milled 5 hours and cold rolled 150 times $TiV_{1.6}Mn_{0.4}$ alloy.

From these X-ray powder diffraction patterns it was determined that the crystallite size of as-cast, milled, and cold rolled samples are respectively 17, 11, and 13 nm [22]. Apart from peak broadening due to the reduction of crystallite size, the pattern of the ball milled sample has the same relative intensities and lattice parameter as the as-cast sample. For the cold rolled sample, the lattice parameter is also the same as the as-cast sample but there is a very strong texture along (200). Texturization is a common feature of cold rolled samples. Neither ball milled sample nor cold rolled sample absorb hydrogen even after 10 cycles of hydrogen pressurization (10 MPa) and vacuum at 423 K. The reason for this significant loss of hydrogen capacity is still not clear.

Figure 8. TEM micrographs of $TiV_{1.6}Mn_{0.4}$ after casting (top), after ball milled for 5 h (middle), and after 150 cold rolls (bottom). Micrographs on the left are bright field images and micrographs on the right are dark field images. From reference [22].

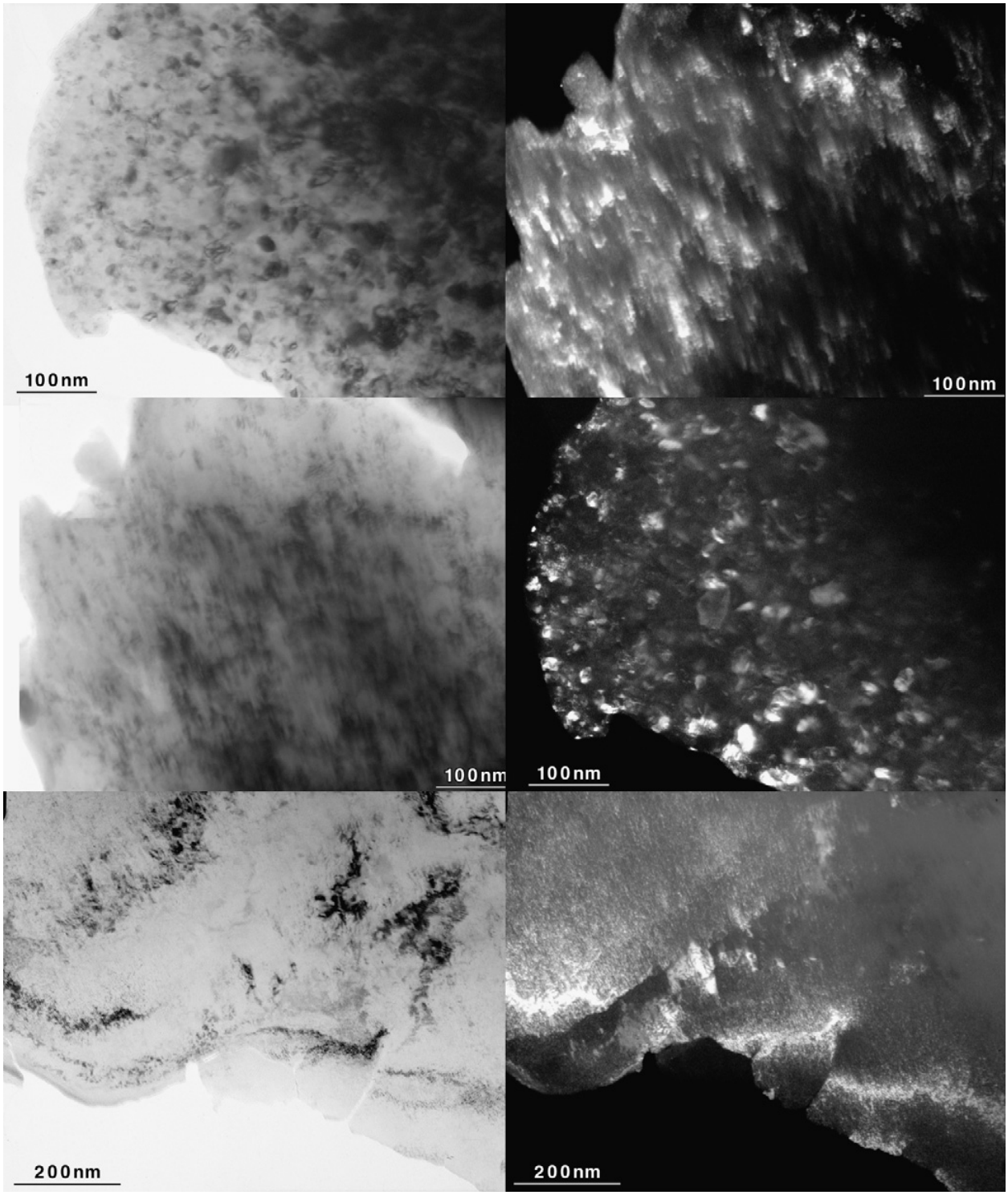

Figure 9. X-ray powder diffraction pattern of arc-melted $TiV_{0.9}Mn_{1.1}$ as a function of milling time. From reference [22].

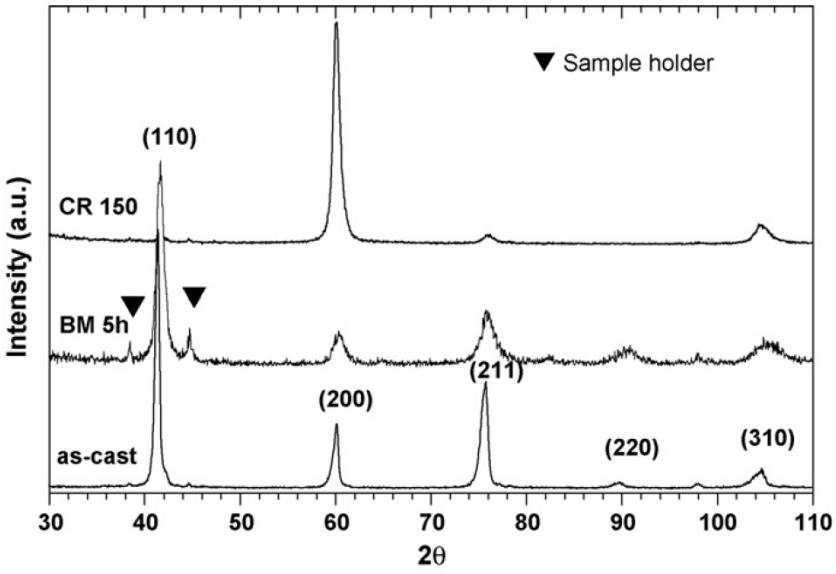

3.2. Mg-Based BCC

Recently, Mg-based BCC alloys have been developed in order to achieve higher hydrogen storage capacity on a weight basis than Ti based ones. In particular, Akiba's group has made an extensive study of the synthesis of Mg–Ti [48,49], Mg–Co [50–52] and Mg–Ni [53,54] BCC alloys by means of ball milling. In this review we will limit our discussion to the Mg–Ti system.

Binary Mg–Ti alloys are being intensively investigated for various applications such as: negative electrodes for Ni–MH batteries, [55,56], H_2 sources for fuel cells [49,57], switchable mirrors for smart solar collectors [58,59], and optical hydrogen detectors [60]. In the phase diagram of the Mg–Ti binary system, equilibrium solid solubility of each metal to another is less than 2 at.% and no intermetallic compound is found. Therefore, non-conventional synthesis methods have to be used. Metastable single-phase Mg–Ti thin films have been successfully synthesized over a large composition range by means of electron-beam and magnetron co-sputter deposition techniques [55,58,59,61,62]. However, these techniques could not be scaled-up to industrial level and other methods have to be investigated. Mechanical alloying has demonstrated its high efficiency for producing metastable Mg–Ti alloys starting from elemental Mg and Ti powders [48,56,63–66].

The synthesis of Mg–Ti BCC alloys by mechanical alloying has been extensively studied by Asano *et al.* [48,49,57,65,66]. Although both Mg and Ti have a hexagonal closed packed (HCP) structure, during milling of a Mg and Ti mixture they react differently. In the case of magnesium, the deformation is mainly by basal plane slip (0001)< −12–10> while for titanium twinning deformation is more important [65]. In one investigation, Asano *et al.* had the idea of adding lithium to magnesium in order to reduce the yield stress of magnesium and also to decreases its lattice parameter [65]. They found that by adding Li to Mg the deformation of Mg was easier and the Ti crystallite size was reduced. These led to a decrease of synthesis time of BCC phase. In a subsequent study, they first synthesized a BCC $Mg_{50}Ti_{50}$ alloy by ball milling a mixture of 50Mg + 50Ti in a Fritsch P5 planetary

ball mill for 150 h at a rotation speed of 200 rpm. Figure 10 confirms that a BCC phase was obtained and from the peaks width a crystallite size of 3 nm was calculated [49].

Figure 10. X-ray diffraction pattern of $Mg_{50}Ti_{50}$ milled for 150 h. From reference [49].

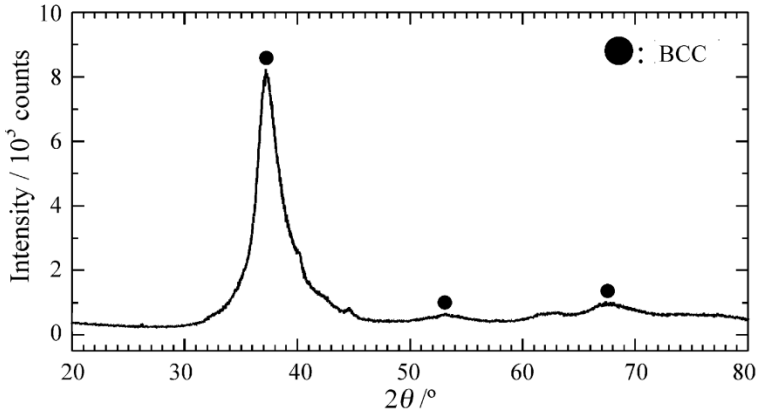

A full hydrogenation at 423 K under 8 MPa of hydrogen and for 122 h resulted in the formation of $Mg_{42}Ti_{58}H_{177}$ FCC hydride phase and some MgH_2.

By controlling milling conditions and Mg:Ti ratio, Asano *et al.* have also shown that BCC, FCC or HCP phase could be obtained in the Mg–Ti system [48]. In the case of HCP phase it is formed by solution of Ti into Mg while the BCC phase is produced by solution of Mg into Ti and the FCC phase is stabilized by introduction of stacking faults in Mg and Ti which have a HCP structure [48,49]. If MgH_2 is used instead of Mg as the starting material then, after ball milling a $50MgH_2 + 50Ti$ mixture the resulting compound is FCC $Mg_{33}Ti_{50}H_{94}$ plus some MgH_2 [57]. The importance of mechanical effect during milling is discussed in reference [66]. It shows that during ball milling of Mg and Ti powders in molar ratio of 1:1, plate-like particles first stuck on the surface of the milling pot and balls. After these plate-like particles fell off from the surface of the milling pot and balls, spherical particles in which concentric layers of Mg and Ti are disposed, are formed. These particles have a mean diameter of 1 mm. These spherical particles are then crushed into spherical particles with diameter of around 10 μm by introduction of cracks along the boundaries between Mg and Ti layers. Finally, the $Mg_{50}Ti_{50}$ BCC phase with a lattice parameter of 0.342(1) nm and a grain size of 3 nm is formed. During milling, Ti acts as an abrasive for Mg which had stuck on the surface of the milling pot and balls [66].

Recently, Çakmak *et al.* showed that mechanical milling of Mg–10 vol.% Ti yields large Mg agglomerate, 90–100 μm, with embedded Ti fragments of about 1 μm uniformly distributed within the agglomerates [67]. These Mg agglomerates are made of coherently diffracting volumes of small size (crystallites). These crystallites, as determined with X-ray diffraction analysis, can be as small as 26 nm after 30 h of milling.

In an investigation of high energy milling of 50Mg–50Ti mixture, Maweja *et al.* observed twinning in Ti-rich crystallites at intermediate milling time [68]. They attributed the twinning to the deformation of Ti particles. But they also pointed out that in the Mg–Ti system it might also indicate a strain induced martensitic transformation of the metastable ω-FCC into BCC. The crystallite boundaries

acted as preferential sites for the heterogeneous nucleation of the twins and for the formation of solid solution by release of the lattice strain energy [68].

For electrochemical applications, mechanical alloyed Mg–Ti materials must be activated by adding of few at.% of Pd. Rousselot *et al.* have shown that if a 50Mg–50Ti mixture is premilled before adding Pd then The alloying of Pd with pre-milled $Mg_{50}Ti_{50}$ occurs very rapidly (few minutes) and is complete after 5 h of milling [69]. They also found that the crystalline structure of the $Mg_{50}Ti_{50}$ alloy (bcc and hcp Mg–Ti phase mixture) does not change significantly with the addition of Pd.

4. Conclusions

Mechanical milling and severe plastic deformation are valuable methods for the synthesis and preparation of nanocrystalline metal hydrides. By far, the most investigated method is mechanical milling. It has been extensively studied as a mean to synthesize intermetallic compounds as well as producing nanocrystalline structures. Mechanical milling effects could be enhanced by changing parameters such as milling atmosphere (reactive milling), temperature, addition of anti-sticking agents, *etc*. This level of sophistication led to impressive results in enhancement of hydrogen storage properties of some metal hydrides by the use of mechanical milling. The next challenge is to scale-up this technology to industrial levels. Here the main hurdle may be the high energy milling which is most usually needed for improving metal hydride properties. This imposes additional requirements in term of specific energy of the milling machine and size of batches that could be processed. These problems are compounded if the milling has to be performed under hydrogen pressure and at high temperature. One also has to take into account the safety aspect of handling metal hydrides. The engineering aspects of these problems could surely be solved. The main challenge will be to keep the capital and operation cost low in order to make the technology competitive. Some SPD techniques such as ECAP and HPT could face the same and maybe bigger scaling-up problems but others, for instance, cold rolling, forging, and extrusion could be more easily adopted by the industry.

In the case of Severe Plastic Deformation, the level of understanding the impact of these techniques on the hydrogen storage properties of metal hydrides is still relatively small. Only a limited number of papers have been published and just a few research groups are investigating metal hydrides applications of SPD. However, first results are encouraging and show similarities with mechanical milling in the effectiveness of obtaining a nanocrystalline structure. Cold rolling and mechanical milling have been shown to have similar effect on hydrogen storage properties: either positive as for example in magnesium-based alloys or negative as for $TiV_{0.9}Mn_{1.1}$ alloy.

From a more fundamental point of view, both mechanical milling and SPD could produce materials with new characteristics such as nanocrystalline structure, metastable phases, high number of defects, texture, important microstrain, etc. Each of these features could have an impact on the hydrogen storage behavior but the exact mechanism is usually not fully understood. More studies on the basic mechanism of mechanical effect through milling and SPD within the scope of hydrogen storage are needed.

Acknowledgement

The author would like to thanks The Research Council of Norway for additional funding that permitted a sabbatical leave at the Institute for Energy Technology (IFE) in Norway.

References

1. Benjamin, J.S. Mechanical alloying. *Sci. Am.* **1976**, *235*, doi:10.1063/1.94213.
2. Suryanarayana, C. Recent developments in mechanical alloying. *Rev. Adv. Mater. Sci.* **2008**, *18*, 203–211.
3. Zhilyaev, A.P.; Langdon, T.G. Using high-pressure torsion for metal processing: Fundamentals and applications. *Prog. Mater. Sci.* **2008**, *53*, 893–979.
4. Vorhauer, A.; Pippan, R. On the homogeneity of deformation by high pressure torsion. *Scr. Mater.* **2004**, *51*, 921–925.
5. Kusadome, Y.; Ikeda, K.; Nakamori, Y.; Orimo, S.; Horita, Z. Hydrogen storage capability of $MgNi_2$ processed by high pressure torsion. *Scr. Mater.* **2007**, *57*, 751–753.
6. Leiva, D.R.; Jorge, A.M.; Ishikawa, T.T.; Huot, J.; Fruchart, D.; Miraglia, S.; Kiminami, C.S.; Botta, W.J. Nanoscale grain refinement and H-sorption properties of MgH_2 processed by high-pressure torsion and other mechanical routes. *Adv. Eng. Mater.* **2010**, *112*, 786–792.
7. Huot, J.; Swainson, I.; Schulz, R. Phase transformation in magnesium hydride induced by ball milling. *Ann. Chim. Sci. Mat.* **2006**, *31*, 135–144.
8. Lima, G.F.; Jorge, A.M.; Leiva, D.R.; Kiminami, C.S.; Bolfarini, C.; Botta, W.J. Severe plastic deformation of Mg–Fe powders to produce bulk hydrides. In *Proceedings of the 13th International Conference on Rapidly Quenched and Metastable Materials*; Dresden, Germany, 24–29 August 2008; Schultz, L., Eckert, J., Battezzati, L., Stoica, M., Eds.; Iop Publishing: Bristol, UK, 2009; Volume 144, No. 012015.
9. Révész, Á.; Kánya, Z.; Verebélyi, T.; Szabó, P.J.; Zhilyaev, A.P.; Spassov, T. The effect of high-pressure torsion on the microstructure and hydrogen absorption kinetics of ball-milled $Mg_{70}Ni_{30}$. *J. Alloy. Compd.* **2010**, *504*, 83–88.
10. Valiev, R.; Langdon, T.G. Principles of equal-channel angular pressing as a processing tool for grain refinement. *Prog. Mater. Sci.* **2006**, *51*, 881–981.
11. Langdon, T.G. The characteristic of grain refinement in materials processed by severe plastic deformation. *Rev. Adv. Mater. Sci.* **2006**, *13*, 6–14.
12. Huang, C.X.; Yang, H.J.; Wu, S.D.; Zhang, Z.F. Microstructural characterizations of Cu processed by ECAP from 4 to 24 passes. *Mater. Sci. Forum* **2008**, *584–586*, 333–337.
13. Skripnyuk, V.; Rabkin, E.; Estrin, Y.; Lapovok, R. The effect of ball milling and equal channel angular pressing on hydrogen absorption/desorption properties of Mg–4.95 wt% Zn–0.71 wt% Zr (ZK60) alloy. *Acta Mater.* **2004**, *52*, 405–414.
14. Skripnyuk, V.; Buchman, E.; Rabkin, E.; Estrin, Y.; Popov, M.; Jorgensen, S. The effect of equal channel angular pressing on hydrogen storage properties of a eutectic Mg–Ni alloy. *J. Alloy. Compd.* **2007**, *436*, 99–106.

15. Skripnyuk, V.M.; Rabkin, E.; Estrin, Y.; Lapovok, R. Improving hydrogen storage properties of magnesium based alloys by equal channel angular pressing. *Int. J. Hydrog. Energy* **2009**, *34*, 6320–6324.
16. Skripnyuk, V.M.; Rabkin, E.; Bendersky, L.A.; Magrez, A.; Carreño-Morelli, E.; Estrin, Y. Hydrogen storage properties of as-synthesized and severely deformed magnesium—Multiwall carbon nanotubes composite. *Int. J. Hydrog. Energy* **2010**, *35*, 5471–5478.
17. Løken, S.; Solberg, J.K.; Maehlen, J.P.; Denys, R.V.; Lototsky, M.V.; Tarasov, B.P.; Yartys, V.A. Nanostructured Mg–Mm–Ni hydrogen storage alloy: Structure-properties relationship. *J. Alloy. Compd.* **2007**, *446–447*, 114–120.
18. Krystian, M.; Zehetbauer, M.J.; Kropik, H.; Mingler, B.; Krexner, G. Hydrogen storage properties of bulk nanostructured ZK60 Mg alloy processed by equal channel angular pressing. *J. Alloy. Compd.* **2011**, *509*, S449–S455.
19. Zhang, L.T.; Ito, K.; Vasudevan, V.K.; Yamaguchi, M. Hydrogen absorption and desorption in a B2 single-phase Ti–22Al–27Nb alloy before and after deformation. *Acta Mater.* **2001**, *49*, 751–758.
20. Zhang, L.T.; Ito, K.; Vasudevan, V.K.; Yamaguchi, M. Effects of cold-rolling on the hydrogen absorption/desorption behavior of Ti–22Al–27Nb alloys. *Mater. Sci. Eng. A* **2002**, *329–331*, 362–366.
21. Patselov, A.M.; Rybin, V.V.; Greenberg, B.A.; Mushnikov, N.V. Hydrogen absorption in as-cast bcc single-phase Ti–Al–Nb alloys. *J. Alloy. Compd.* **2010**, *505*, 183–187.
22. Couillaud, S.; Enoki, H.; Amira, S.; Bobet, J.L.; Akiba, E.; Huot, J. Effect of ball milling and cold rolling on hydrogen storage properties of nanocrystalline $TiV_{1.6}Mn_{0.4}$ alloy. *J. Alloy. Compd.* **2009**, *484*, 154–158.
23. Amira, S.; Santos, S.F.; Huot, J. Hydrogen sorption properties of Ti–Cr alloys synthesized by ball milling and cold rolling. *Intermetallics* **2010**, *18*, 140–144.
24. Ueda, T.T.; Tsukahara, M.; Kamiya, Y.; Kikuchi, S. Preparation and hydrogen storage properties of Mg–Ni–Mg_2Ni laminate composites. *J. Alloy. Compd.* **2004**, *386*, 253–257.
25. Pedneault, S.; Huot, J.; Roué, L. Nanostructured Mg_2Ni materials prepared by cold rolling and used as negative electrode for Ni–MH batteries. *J. Power Sources* **2008**, *185*, 566–569.
26. Pedneault, S.; Roué, L.; Huot, J. Synthesis of metal hydrides by cold rolling. *Mater. Sci. Forum* **2008**, *570*, 33–38.
27. Dufour, J.; Huot, J. Rapid activation, enhanced hydrogen sorption kinetics and air resistance in laminated Mg–Pd 2.5 at.% *J. Alloy. Compd.* **2007**, *439*, L5–L7.
28. Takeichi, N.; Tanaka, K.; Tanaka, H.; Ueda, T.T.; Kamiya, Y.; Tsukahara, M.; Miyamura, H.; Kikuchi, S. The hydrogen storage properties of Mg/Cu and Mg/Pd laminate composites and metallographic structure. *J. Alloy. Compd.* **2007**, *446–447*, 543–548.
29. Dufour, J.; Huot, J. Study of Mg_6Pd alloy synthesized by cold rolling. *J. Alloy. Compd.* **2007**, *446–447*, 147–151.
30. Mori, R.; Miyamura, H.; Kikuchi, S.; Tanaka, K.; Takeichi, N.; Tanaka, H.; Kuriyama, N.; Ueda, T.T.; Tsukahara, M. Hydrogenation characteristics of Mg based alloy prepared by super lamination technique. *Mater. Sci. Forum* **2007**, *561–565*, 1609–1612.

31. Danaie, M.; Mauer, C.; Mitlin, D.; Huot, J. Hydrogen storage in bulk Mg–Ti and Mg–stainless steel multilayer composites synthesized via accumulative roll-bonding (ARB). *Int. J. Hydrog. Energy* **2011**, *36*, 3022–3036.
32. Suganuma, K.; Miyamura, H.; Kikuchi, S.; Takeichi, N.; Tanaka, K.; Tanaka, H.; Kuriyama, N.; Ueda, T.T.; Tsukahara, M. Hydrogen storage properties of Mg-Al alloy prepared by super lamination technique. *Adv. Mater. Res.* **2007**, *26–28*, 857–860.
33. Tanaka, K.; Takeichi, N.; Tanaka, H.; Kuriyama, N.; Ueda, T.T.; Tsukahara, M.; Miyamura, H.; Kikuchi, S. Investigation of micro-structural transition through disproportionation and recombination during hydrogenation and dehydrogenation in Mg/Cu super-laminates. *J. Mater. Sci.* **2008**, *43*, 3812–3816.
34. Leiva, D.R.; Fruchart, D.; Bacia, M.; Girard, G.; Skryabina, N.; Villela, A.C.S.; Miraglia, S.; Santos, D.S.; Botta, W.J. Mg alloy for hydrogen storage processed by SPD. *Int. J. Mater. Res.* **2009**, *100*, 1739–1746.
35. Wang, J.-Y.; Wu, C.-Y.; Nieh, J.-K.; Lin, H.-C.; Lin, K.M.; Bor, H.-Y. Improving the hydrogen absorption properties of commercial Mg-Zn-Zr alloy. *Int. J. Hydrog. Energy* **2010**, *35*, 1250–1256.
36. Fukai, Y. The Metal-hydrogen system. In *Springer Series in Materials Science*, 2nd ed.; Springer-Verlag: Berlin, Germany, 2005; Volume 21, p. 497.
37. Akiba, E.; Okada, M. Metallic hydrides III: Body-centered-cubic solid-solution alloys. *MRS Bull.* **2002**, *27*, 699–703.
38. Nakamura, Y.; Akiba, E. Hydriding properties and crystal structure of NaCl-type mono-hydrides formed from Ti–V–Mn BCC solid solutions. *J. Alloy. Compd.* **2002**, *345*, 175–182.
39. Kubo, K.; Itoh, H.; Takahashi, T.; Ebisawa, T.; Kabutomori, T.; Nakamura, Y.; Akiba, E. Hydrogen absorbing properties and structures of Ti–Cr–Mo alloys. *J. Alloy. Compd.* **2003**, *356–357*, 452–455.
40. Iwase, K.; Nakamura, Y.; Mori, K.; Harjo, S.; Ishigaki, T.; Kamiyama, T.; Akiba, E. Hydrogen absorption-desorption properties and crystal structure analysis of Ti–Cr–Mo alloys. *J. Alloy. Compd.* **2005**, *404–406*, 99–102.
41. Shibuya, M.; Nakamura, J.; Akiba, E. Hydrogenation properties and microstructure of Ti–Mn-based alloys for hybrid hydrogen storage vessel. *J. Alloy. Compd.* **2008**, *466*, 558–562.
42. Shibuya, M.; Nakamura, J.; Enoki, H.; Akiba, E. High-pressure hydrogenation properties of Ti–V–Mn alloy for hybrid hydrogen storage vessel. *J. Alloy. Compd.* **2009**, *475*, 543–545.
43. Yu, X.B.; Wu, Z.; Xia, B.J.; Xu, N.X. Improvement of activation performance of quenched Ti–V-based BCC phase alloys. *J. Alloy. Compd.* **2004**, *386*, 258–260.
44. Huot, J.; Enoki, H.; Akiba, E. Synthesis, phase transformation, and hydrogen storage properties of ball-milled $TiV_{0.9}Mn_{1.1}$. *J. Alloy. Compd.* **2008**, *453*, 203–209.
45. Eckert, J.; Holzer, J.C.; Krill, C.E., III; Johnson, W.L. Mechanically driven alloying and grain size changes in nanocrystalline Fe–Cu powders. *J. Appl. Phys.* **1992**, *73*, 2794–2802.
46. Santos, S.F.; Costa, A.L.M.; de Castro, J.F.R.; dos Santos, D.S.; Botta, W.J.; Ishikawa, T.T. Mechanical and reactive miling of a TiCrV BCC solid solution. *J. Metastable Nanocrystalline Mater.* **2004**, *20–21*, 291–296.
47. Singh, B.K.; Shim, G.; Cho, S.-W. Effects of mechanical milling on hydrogen storage properties of $Ti_{0.32}Cr_{0.43}V_{0.25}$ alloy. *Int. J. Hydrog. Energy* **2007**, *32*, 4961–4965.

48. Asano, K.; Enoki, H.; Akiba, E. Synthesis of HCP, FCC and BCC structure alloys in the Mg–Ti binary system by means of ball milling. *J. Alloy. Compd.* **2009**, *480*, 558–563.
49. Asano, K.; Enoki, H.; Akiba, E. Synthesis of Mg–Ti FCC hydrides from Mg–Ti BCC alloys. *J. Alloy. Compd.* **2009**, *478*, 117–120.
50. Zhang, Y.; Tsushio, Y.; Enoki, H.; Akiba, E. The hydrogen absorption-desorption performances of Mg–Co–X ternary alloys with BCC structure. *J. Alloy. Compd.* **2005**, *393*, 185–193.
51. Zhang, Y.; Tsushio, Y.; Enoki, H.; Akiba, E. The study on binary Mg–Co hydrogen storage alloys with BCC phase. *J. Alloy. Compd.* **2005**, *393*, 147–153.
52. Shao, H.Y.; Asano, K.; Enoki, H.; Akiba, E. Fabrication, hydrogen storage properties and mechanistic study of nanostructured $Mg_{50}Co_{50}$ body-centered cubic alloy. *Scr. Mater.* **2009**, *60*, 818–821.
53. Shao, H.; Asano, K.; Enoki, H.; Akiba, E. Preparation and hydrogen storage properties of nanostructured Mg–Ni BCC alloys. *J. Alloy. Compd.* **2009**, *477*, 301–306.
54. Shao, H.; Asano, K.; Enoki, H.; Akiba, E. Fabrication and hydrogen storage property study of nanostructured Mg–Ni–B ternary alloys. *J. Alloy. Compd.* **2009**, *479*, 409–413.
55. Niessen, R.A.H.; Notten, P.H.L. Electrochemical hydrogen storage characteristics of thin film MgX (X = Sc, Ti, V, Cr) compounds. *Electrochem. Solid State Lett.* **2005**, *8*, A534–A538.
56. Kalisvaart, W.P.; Notten, P.H.L. Mechanical alloying and electrochemical hydrogen storage of Mg-based systems. *J. Mater. Res.* **2008**, *23*, 2179–2187.
57. Asano, K.; Akiba, E. Direct synthesis of Mg–Ti–H FCC hydrides from MgH_2 and Ti by means of ball milling. *J. Alloy. Compd.* **2009**, *481*, L8–L11.
58. Borsa, D.M.; Baldi, A.; Pasturel, M.; Schreuders, H.; Dam, B.; Griessen, R.; Vermeulen, P.; Notten, P.H.L. Mg–Ti–H thin films for smart solar collectors. *Appl. Phys. Lett.* **2006**, *88*, doi:10.1063/1.2212287.
59. Borsa, D.M.; Gremaud, R.; Baldi, A.; Schreuders, H.; Rector, J.H.; Kooi, B.; Vermeulen, P.; Notten, P.H.L.; Dam, B.; Griessen, R. Structural, optical, and electrical properties of $Mg_yTi_{1-y}H_x$ thin films. *Phys. Rev. B* **2007**, *75*, doi:10.1103/PhysRevB.75.205408.
60. Slaman, M.; Dam, B.; Schreuders, H.; Griessen, R. Optimization of Mg-based fiber optic hydrogen detectors by alloying the catalyst. *Int. J. Hydrog. Energy* **2008**, *33*, 1084–1089.
61. Vermeulen, P.; Niessen, R.A.H.; Notten, P.H.L. Hydrogen storage in metastable $Mg_yTi_{(1-y)}$ thin films. *Electrochem. Commun.* **2006**, *8*, 27–32.
62. Vermeulen, P.; van Thiel, E.F.M.J.; Notten, P.H.L. Ternary $MgTi_X$-alloys: A promising route toward low-temperature, high-capacity, hydrogen-storage materialsthin films. *Chem. Eur. J.* **2007**, *13*, 9892–9898.
63. Rousselot, S.; Bichat, M.P.; Guay, D.; Roué, L. Structure and electrochemical behaviour of metastable $Mg_{50}Ti_{50}$ alloy prepared by ball milling. *J. Power Sources* **2008**, *175*, 621–624.
64. Rousselot, S.; Guay, D.; Roué, L. Synthesis of fcc Mg–Ti–H alloys by high energy ball milling: Structure and electrochemical hydrogen storage properties. *J. Power Sources* **2010**, *195*, 4370–4374.
65. Asano, K.; Enoki, H.; Akiba, E. Effect of Li addition on synthesis of Mg–Ti BCC alloys by means of ball milling. *Mater. Trans. JIM* **2007**, *48*, 121–126.

66. Asano, K.; Enoki, H.; Akiba, E. Synthesis process of Mg–Ti BCC alloys by means of ball milling. *J. Alloy. Compd.* **2009**, *486*, 115–123.
67. Çakmak, G.; Károly, Z.; Mohai, I.; Öztürk, T.; Szépvölgyi, J. The processing of Mg–Ti for hydrogen storage; mechanical milling and plasma synthesis. *Int. J. Hydrog. Energy* **2010**, *35*, 10412–10418.
68. Maweja, K.; Phasha, M.; van der Berg, N. Microstructure and crystal structure of an equimolar Mg–Ti alloy processed by Simoloyer high-energy ball mill. *Powder Technol.* **2010**, *199*, 256–263.
69. Rousselot, S.; Gazeau, A.; Guay, D.; Roué, L. Influence of Pd on the structure and electrochemical hydrogen storage properties of Mg50Ti50 alloy prepared by ball milling. *Electrochim. Acta* **2010**, *55*, 611–619.